LightRider: Reliable UAV Ground Communication with a Single Laser Tethering Link

Junjie Wang[ℙ], Kenuo Xu[ℙ], Zhe Ou[𝕁], Zhaofeng Luo[ℂ], Bo Liang[ℙ], Muhan Li[ℙ],
Xiaoming Liu[ℙ], Lingyang Song[ℙ], Guobin Shen[ℍ], Xinwei Yao[ℤ✉], Chenren Xu[ℙ𝕂✉]
[ℙ]Peking University [𝕁]Johns Hopkins University [ℂ]Carnegie Mellon University
[ℍ]The Hong Kong University of Science and Technology (Guangzhou) [ℤ]Zhejiang University of Technology
[𝕂]Key Laboratory of High Confidence Software Technologies, Ministry of Education (PKU)
Email: junjiewang25@stu.pku.edu.cn, kenuo.xu@pku.edu.cn, zou6@jhu.edu, zhaofen2@andrew.cmu.edu,
rambo@pku.edu.cn, muhan@stu.pku.edu.cn, harry.python@gmail.com, lingyang.song@pku.edu.cn,
guobinshen@hkust-gz.edu.cn, xwyao@zjut.edu.cn[✉], chenren.xu@gmail.com[✉]

***Abstract*—Unmanned aerial vehicles (UAVs) are increasingly vulnerable to electromagnetic interference (EMI) in their communication and networking systems, posing significant risks to mission success and operational safety. To address the limitations of radio frequency (RF) communication in such scenarios, we propose a reliable laser-based communication system for UAV operations in EMI-prone environments. Our system features a single laser tethering link (*i.e.*, ensuring the laser beam continuously illuminates a moving UAV) that simultaneously enables laser tracking, alignment, and communication. Leveraging the optical properties of laser beams and retroreflectors, the laser tethering design utilizes a photodiode (PD) array to detect and calculate the precise position of the beam spot from a distance. We further design a beam alignment control algorithm that maintains continuous optical tethering using only the single, narrow laser beam. Our design effectively eliminates the need for RF-based position feedback (as conventional tethering design needed) that could be vulnerable to EMI interference. To minimize the interference between tethering and communication functions, we further design a beam spot prediction algorithm coupled with modulation, which compensates for the inevitable impact of modulation on the continuity of tethering. Experimental evaluation using our prototype demonstrates a maximum tethering distance of 150 meters and communication distances of 380 meters. The system successfully tracks UAVs moving at angular velocities up to 57°/s and maintains functionality in the presence of commercial UAV jammers. A demonstration video showcasing the system's operation is available at https://youtu.be/rAFIpUadkOc.**

***Index Terms*—Electromagnetic Interference, Free-Space Optical Communication, Unmanned Aerial Vehicles**

ACKNOWLEDGMENT

We thank the anonymous reviewers for their insightful comments and suggestions. This work is supported by National Key Research and Development Plan, China (Grant No. 2023YFB2903902), the National Natural Science Foundation of China (Grant No. U25B2040, 62272010), and the "Pioneer" and "Leading Goose" R&D Program of Zhejiang (Grant No. 2025C01054, No. 2024C03274). Chenren Xu and Xinwei Yao are the corresponding authors.

I. INTRODUCTION

The rapid application of Unmanned Aerial Vehicles (UAVs) into diverse applications [1], [2] has been accompanied by an increasing number of safety concerns and accidents [3], [4]. A significant portion of these issues stems from the vulnerability of radio frequency (RF)-based wireless communication systems to environmental electromagnetic interference (EMI). Current RF communication systems for UAVs are highly susceptible to interference from various sources, including not only environmental factors like high-voltage power lines and cellular base stations, but also intentional malicious attacks from UAV jammers [5]. Such interference significantly degrades the reliability of communication, leading to command delays that hinder mission execution or even catastrophic crashes [6]. These challenges highlight the urgent need for reliable and EMI-resistant communication networks, which are crucial for ensuring the safe and widespread adoption of UAV technology in real-world scenarios.

Current approaches, such as frequency-hopping spread spectrum [7] and spectrum sensing [8], are able to provide protection against mild interference in RF-based UAV communication systems primarily. However, they prove ineffective against more severe disturbances such as intentional jamming attacks [9]. Alternative solutions have explored the use of optical [10] and acoustic [11] communication. However, these approaches face significant limitations: ambient interference and restricted transmission power result in operational ranges typically below 10 meters, rendering them impractical for most real-world applications [12]. Another real-world solution involves the use of fiber-optic technology, where a lightweight fiber is tethered to the UAV for EMI-resistant data transmission to the ground [13]. Although this method effectively eliminates EMI concerns, it introduces significant operational limitations. The fragile tether severely restricts the UAV's maneuverability and reliability [14]. These limitations highlight the need for a more reliable solution that combines EMI resistance with operational flexibility for UAV communication systems.

In this paper, we pose the research question: can laser communication technology enable a reliable, long-range, and EMI-resistant communication system for UAV operations? Laser-based wireless communication, often referred to as free-space optical (FSO) communication, has demonstrated the potential for long-distance transmission in free space [15]. However, unlike conventional mobile platforms, UAVs impose distinct requirements that render existing FSO solutions inadequate. Here, we identify three critical specifications for reliable UAV-FSO systems beyond existing mobile FSO systems:

• *Complete EMI immunity.* Existing laser systems for mobile devices typically rely on a RF-based feedback channel to transmit target position data to the ground station, enabling the laser transmitter to adjust its beam direction accordingly [16]. However, this architecture fundamentally compromises EMI resistance as RF-dependent channels are inherently vulnerable to EMI disruption. Therefore, FSO systems in UAV scenarios require a fully optical tracking mechanism to ensure operational robustness in EMI-intensive environments.

• *Extended operational range.* Our tethering system must provide a sufficiently long working distance to fully leverage the inherent range advantages of laser communication. However, optical signals are highly susceptible to ambient noise. Conventional light sources (*e.g.,* LEDs) and receivers (*e.g.,* RGB or infrared cameras) with large divergence angles experience significant signal attenuation over relatively short distances (*e.g.,* only usable at ranges below 10 meters [17]). This limitation stems from the rapid dispersion of non-collimated light. We argue that only highly focused laser beams, can achieve the necessary range to meet the demands of practical UAV tethering.

• *Ultra-responsive tracking.* While the highly directional nature of laser beams enables long distance, it simultaneously introduces significant challenges for *tethering using such a narrow beam*. A critical issue arises when a UAV moves out of the beam's coverage between two consecutive observations, leading to signal loss and subsequent tethering failure. To mitigate this, the tethering system must achieve both a sufficiently high sampling rate and a low alignment execution delay. These requirements are essential to support the high mobility of UAVs, ensuring that the beam can continuously adapt to rapid positional changes.

Our study begins by addressing the fundamental challenge of establishing a precise feedback loop without relying on vulnerable RF channels or slow computer vision methods. While corner-cube retroreflectors are commonly used for simply reflecting a beam [18], we unveil an underutilized property: they strictly preserve the spatial profile of the reflected laser beam relative to the incidence offset. This unique property allows us to infer the UAV's position solely by analyzing the retro-reflected beam's displacement at the laser transmitter. Leveraging this insight, we design a specific photodiode (PD) array to capture these spatial patterns, enabling the transmitter to track the UAV continuously and precisely through the laser link itself.

To realize this single-laser tethering in dynamic environments, we address three critical design challenges regarding sensing resolution, signal integrity, and functional conflict: (1) *Reconciling spatial and temporal resolution:* High-mobility tethering requires microsecond-level feedback that standard cameras cannot provide, while single photodiodes lack necessary spatial information. We design a *fully parallel PD array* that samples spatially distributed intensity simultaneously, achieving high temporal resolution for real-time deviation detection. (2) *Overcoming optical power loss:* Long-distance sensing is strictly limited by signal attenuation, yet conventional optical systems use beam splitters that inherently waste significant optical power. We propose a *coaxial optical design* that arranges the PD array around the emitter, eliminating beam splitters to maximize the received signal for extended range. (3) *Mitigating tethering disruptions from communication:* The modulation schemes (*i.e.,* On-Off Keying) necessitate turning the laser off to transmit data, which inherently disrupts the continuous optical feedback loop required for tracking. We design a *motion prediction algorithm* to compensate for these signal gaps, ensuring stable tethering even during modulation-induced interruptions.

We develop a prototype, LIGHTRIDER, comprising a ground-based Anchor and a lightweight (58.5 g) UAV Node. Extensive real-world experiments demonstrate that LIGHTRIDER supports angular velocities up to 57°/s and maintains stable tethering at 150 m. Crucially, in the presence of two 30 W commercial jammers that paralyze standard UAV controls, LIGHTRIDER maintains robust communication up to 380 m. Furthermore, emulation based on real-world metrics indicates that with upgraded optical components, the system design can potentially scale to an operational range of 1200 meters. A demonstration video showcasing the system's operation is available at https://youtu.be/rAFIpUadkOc.

Contributions.

- We present LIGHTRIDER, the first laser-based system capable of supporting long-distance, fully mobile (tethering/tracking and) communication that relies solely on one single laser link.
- We propose a fully optical laser tethering mechanism, combining innovative optical, electrical, and algorithmic designs to enable robust and continuous mobile laser tethering over a distance without relying on side channel (*e.g.,* RF and computer vision) feedback.
- We develop a prototype and conduct real-world evaluations to demonstrate its ability to support reliable tethering and communication at distances exceeding 150 meters in the presence of strong EMI.

This work does not raise any ethical issues. We also ensure that no nearby device is affected or attempting to communicate with our testbed.

II. BACKGROUND

Laser Communication Primer. Communication using laser in the open space, typically referred to as Free-Space Optical (FSO) communication, is a wireless technology that employs optical carrier signals (*e.g.,* visible light) for data transmission through unguided propagation media (*e.g.,* the atmosphere rather than optical fibers) [19]. A typical FSO system includes a transmitter with a light source, modulator, and beam-forming optics, and a receiver that uses a photodiode to convert the

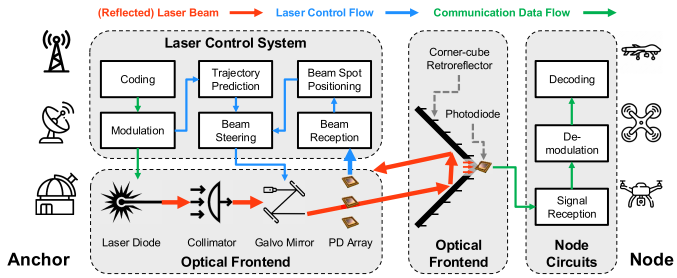

Fig. 1: LIGHTRIDER.

received light to electrical signals for subsequent processing and demodulation.

Modeling of Laser Beam. The spatial intensity distribution of laser beams during propagation can be characterized using Gaussian beam theory [20], mathematically described by:

$$I(r,z) = \frac{I_0}{1 + z^2/z_0^2} e^{-2(r/w)^2} \tag{1}$$

where $I(r,z)$ represents the optical intensity at radial distance r from the beam axis and propagation distance z from the beam's narrowest point, I_0 denotes the peak intensity at the beam center, z_0 characterizes the beam divergence, and w describes the beam width at distance z. Notably, the Gaussian property remains invariant under multiple mirror reflections.

III. SYSTEM OVERVIEW

As illustrated in Fig. 1, LIGHTRIDER consists of a ground Anchor and an airborne Node. The Anchor steers a laser with a two-axis galvo mirror, senses the retroreflected beam with a PD array, and transmits downlink data. The lightweight Node integrates a corner-cube retroreflector, a central PD, and control circuitry. During operation, the retroreflected beam provides positional feedback to the Anchor, which closes the tracking loop and maintains tethering while the same beam carries communication.

Laser Tethering. The laser tethering mechanism enables continuous tracking and beam alignment with a UAV during random mobility. The Node's corner-cube reflector preserves the spatial characteristics of the incident beam, allowing the Anchor to detect positional deviations by analyzing the reflected beam spot pattern (§IV-A). The Anchor incorporates a PD array to detect this spatial deviation (§IV-B). The deviation serves as the input for the beam steering control algorithm, which dynamically adjusts the galvo mirror for continuous laser beam alignment towards the Node in real time (§IV-C).

Integrated Communication with Tethering. LIGHTRIDER includes communication links that integrates with the laser tethering mechanism. The Anchor employs standard On-Off Keying (OOK, with Manchester coding) modulation, while the Node utilizes its photodiode for signal reception and decoding. To mitigate interference between communication and tethering, the system adopts a predictive beam position estimation algorithm that maintains tethering continuity during laser-off periods (§IV-D).

IV. LIGHTRIDER DESIGN

Achieving a single-laser optical tethering system presents two challenges: (1) establishing an optical feedback mechanism for position and deviation detection over long distances, and (2) maintaining tethering stability during high-speed UAV maneuvers. To address these challenges, we first investigate the unique properties of a corner-cube retroreflector in the Node, which preserves reflected beam spot characteristics. Subsequently, we leverage a high-speed PD array at the Anchor to capture beam spot patterns with microsecond-level temporal resolution for real-time deviation detection. We further design a beam steering control algorithms using the calculated beam spot deviation, forming a closed-loop tethering system that maintains robust optical connectivity with highly mobile UAVs using only a single laser beam. Finally, through in-depth analysis of the communication process, we minimize the interference of communication on tethering by carefully selecting modulation schemes and designing a beam spot prediction algorithm.

A. Beam Position Feedback with Retroreflector

In order to enable precise laser tethering at the Anchor, a fundamental requirement is the accurate determination of the current beam alignment accuracy. This necessitates a feedback mechanism in which the laser beam spot position information is returned from the Node to the Anchor. We achieve this by leveraging a geometric property of corner-cube retroreflectors. While retroreflectors are generally known for reflecting light back toward its source, we observe that a corner-cube does not return the beam to exactly the same position. Instead, it introduces a subtle but deterministic shift in the reflected laser spot, which can be exploited to infer the Node 's position solely from measurements at the Anchor.

A corner-cube retroreflector consists of three mutually perpendicular reflective surfaces forming the internal corner of a cube. When a laser beam is incident on these surfaces, the multiple reflections are equivalent to light emerging from a virtual point symmetric to the corner-cube center, and the outgoing direction is opposite to that of the incident beam. As illustrated in Fig. 2, if the lateral offset between the incident beam and the corner-cube center is denoted by δ, then, after reflection, the beam spot returning toward the source is shifted to a distance of 2δ from the original incident position. This geometric relationship is independent of the Node 's motion, as long as the beam is successfully retroreflected. As depicted in Fig. 2c, the offset becomes δ' after translation, where δ' denotes the updated lateral offset, and the returning beam spot is shifted to $2\delta'$ accordingly. Consequently, by precisely measuring the position of the returning beam spot at the Anchor, we can recover δ and thereby obtain the Node 's relative position, providing the self-contained feedback required for accurate laser tethering.

B. Beam Spot Positioning at Anchor

To effectively receive the retroreflected laser beam for precise positioning, we design a hollow PD array around the

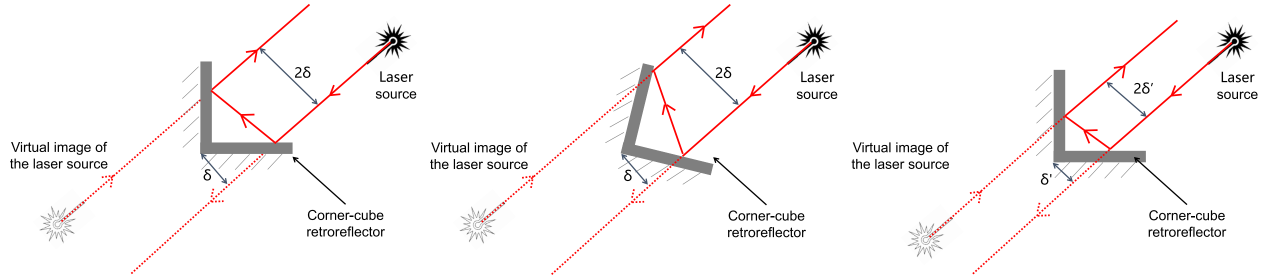

(a) Original reflection. (b) After rotation. (c) After translation.

Fig. 2: Illustrations of optical feedback with retroreflector. We use a 2D representation for simplicity and the property in 3D space is analogous.

laser emission point at the Anchor. This coaxial layout avoids blocking the outgoing beam while allowing multiple densely placed PDs to sample the intensity of the reflected beam for accurate spot localization. As shown in Fig. 4a, our prototype uses 12 photodiodes arranged around a central through-hole that serves as the outgoing laser path.

The laser beam reflected to the Anchor adheres to the Gaussian beam intensity distribution (Eqn. 1). Assume the beam propagation direction as z axis, the intensity distribution for a Gaussian beam on a 2D plane (of the PD array) can be described as follows:

$$I(x,y,z) = I_z \exp\left(-\frac{(x-x_0)^2}{2\sigma_x^2} - \frac{(y-y_0)^2}{2\sigma_y^2}\right) \quad (2)$$

where $I(x,y,z)$ is the intensity detected at the point (x,y,z) and x_0 and y_0 are the coordinates of the center of the beam spot. To determine the center coordinates from the intensity data sampled by the PD array, we first take the natural logarithm of Eqn. 2 and then, by collecting the resulting equations for all n PDs at different positions, obtain a system of equations:

$$\begin{cases} i_1 = ax_1^2 + by_1^2 + cx_1 + dy_1 + e \\ \quad\vdots \\ i_n = ax_n^2 + by_n^2 + cx_n + dy_n + e \end{cases} \quad (3)$$

where $i = \ln I(x,y)$, $a = -\frac{1}{2\sigma_x^2}$, $b = -\frac{1}{2\sigma_y^2}$, $c = \frac{x_0}{\sigma_x^2}$, $d = \frac{y_0}{\sigma_y^2}$ and $e = \ln I_z + \frac{x_0^2}{2\sigma_x^2} + \frac{y_0^2}{2\sigma_y^2}$.

We then solve this system in the least-squares sense to estimate the Gaussian beam parameters, from which the spot center (x_0, y_0) on the PD plane is computed by $x_0 = -\frac{c}{2a}$ and $y_0 = -\frac{d}{2b}$.

C. Real-time Laser Direction Control

To support tethering for high-mobility UAVs, the control loop must achieve a high refresh rate. This requirement arises from the narrow laser beam, which defines only a small detection window: once the Node leaves the optical path, it immediately disappears from the Anchor's detection range, causing complete loss of positional feedback. This vulnerability requires an ultra-responsive control system to maintain continuous tracking under rapid UAV motion. Our design addresses this challenge through a high-speed feedback mechanism that compensates for the maximum anticipated mobility of the Node.

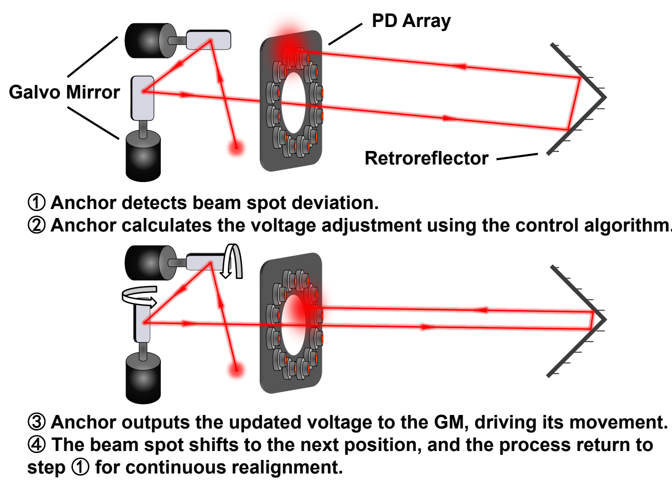

Fig. 3: Workflow of the real-time laser direction control.

The objective of our control algorithm is to keep the reflected beam spot at the center of the PD array. As shown in Fig. 3, the controller takes the beam spot position estimated from the PD array (Eqn. 3) as input and steers the emitted beam using a Galvo Mirror (GM). A typical GM consists of two orthogonal mirrors, each independently rotated by the voltage applied to its motor. Therefore, the controller outputs the voltages for these two mirror axes.

Our control algorithm is fundamentally centered around achieving precise laser alignment through gradual steering based on beam spot deviation. Since the exact distance between the Anchor and the Node cannot be obtained, we are unable to directly calculate the required laser steering angle. Therefore, we employ a step-by-step steering method: after the PD array samples and positions the beam spot center, the direction in which the laser needs to be steered can be determined, and the galvo mirror is then driven to make a slight angular adjustment in that direction. By repeating this process, determining the adjustment direction and making a small angular correction, the laser beam can eventually achieve precise alignment with the Node. Thanks to the high temporal resolution of the PD array and the low-latency response of the galvo mirror, this high-frequency, small-step steering approach enables low-latency precise alignment. However, in scenarios requiring extremely high angular velocity tethering, this step-by-step steering method may lead to insufficient tracking speed due to the small angular step size. At the same time, for completely stationary or low-speed moving targets, large angular step sizes may cause tracking oscillations. To optimize tethering performance, we design a Proportional-Integral-Derivative (PID) controller, which dynamically adjusts the laser steering step size based on the deviation distance of the beam spot center. The PID controller operates on the principle of error correction. Mathematically, the control signal for the n dimension ($n \in \{x, y\}$) PID controller can be expressed as

$$\Delta V_n(t) = K_p \cdot n_0(t) + K_i \int_0^t n_0(\tau) d\tau + K_d \frac{d}{dt} n_0(t), \tag{4}$$

where $\Delta V_x(t)$ and $\Delta V_y(t)$ are the changes in the voltages applied to the two mirrors of GM, and $x_0(t)$ and $y_0(t)$ are the estimated position of reflected beam at each timestamp. K_p, K_i, and K_d are PID controller parameters, which are set to $K_p = 10^{-5}$, $K_i = 10^{-12}$, $K_d = 10^{-8}$ in our prototype. The per-update control output is capped at 0.25 DAC-scale unit to avoid overly aggressive high-frequency galvo actuation. These values are empirically tuned by sequentially adjusting the gains and selecting the setting that yields the highest sustained reflected-beam SNR without loss of tethering.

D. Integrated Communication and Tethering

Although our tethering mechanism effectively maintains laser alignment under continuous laser operation, integrating it with communication introduces a fundamental challenge: modulation-induced laser-off periods disrupt the tethering feedback loop. During these off durations, the absence of reflected light prevents the Anchor from acquiring positional information, creating a vulnerability in the tethering system.

To address the temporary loss of optical feedback during laser-off periods, we integrate a trajectory prediction module into the tethering control loop. During laser-on periods, the system executes the standard beam control described in §IV-C while continuously logging the control voltages $V_x(t)$ and $V_y(t)$ with timestamps t. When the laser switches off for communication, the controller fits a cubic model to the most recent control history and uses it to generate predicted steering commands throughout the off interval.

Specifically, for each dimension $d \in \{x, y\}$, we approximate the control voltage as

$$\hat{V}_d(t) = \alpha_{d0} + \alpha_{d1} t + \alpha_{d2} t^2 + \alpha_{d3} t^3, \tag{5}$$

where the coefficients $\{\alpha_{d0}, \alpha_{d1}, \alpha_{d2}, \alpha_{d3}\}$ are obtained by least-squares fitting over the most recent 16 samples (about 0.2 ms in our prototype). The predicted voltages $\hat{V}_x(t)$ and $\hat{V}_y(t)$ generated by (5) directly drive the beam steering hardware during laser-off periods, enabling continuous tracking without instantaneous PD feedback. This cubic prediction model offers a favorable trade-off between accuracy and computational cost on the resource-constrained microcontroller unit (MCU) and, in our experiments, improves the received SNR during integrated communication and tethering by about 5 dB, with peak gains up to 15 dB, thereby significantly enhancing tethering reliability.

V. IMPLEMENTATION

We fabricate the prototype for both ends of the system: the Anchor and the Node, as illustrated in Fig. 4. The Anchor integrates a tethering subsystem for maintaining the laser link and a communication subsystem for data transmission, while the compact and lightweight Node integrates a passive tethering subsystem and a low-power communication subsystem for data reception.

Anchor. Both Anchor's tethering and communication subsystem are implemented on a circuit board and controlled by an STM32H750 MCU [21] operating at 480 MHz. The tethering subsystem receives feedback from the Node and aligns the laser beam accordingly. Its peripherals include 12 PDs [22] with a 0.3 mm active diameter, uniformly arranged every 30° on a concentric 10.4 mm-radius circle around a 7.8 mm-radius central aperture, a 635 nm narrow-bandpass filter, a central-aperture light shield, a precise amplifier [23], a GM [24], and a collimator [25]. Laser light reflected by the retroreflector generates photocurrent, which is converted to voltage via a transimpedance amplifier and digitized at 500 Ksps by the MCU's 16-bit ADC. The MCU then uses its dual-channel 12-bit DAC to adjust the GM control voltage and steer the laser's emission angle. The communication subsystem uses a 635 nm, 20 dBm laser source driven by the same MCU; for the downlink, the MCU generates Manchester-coded OOK modulation signals and outputs them via GPIO to modulate the laser intensity.

Node. The Node reflects the laser beam and demodulates information from the Anchor. Its optical front-end uses a commercial, uncoated dielectric corner cube retroreflector with a PD placed behind it. *Because the corner cube is glass and uncoated, both total internal reflection and partial transmission occur [26], allowing a small portion of the incident beam to pass through.* The PD signal is amplified by a high-bandwidth amplifier and then processed by an STM32L431CCT6 MCU, which serves as the core demodulation controller.

VI. EVALUATION

To comprehensively evaluate LIGHTRIDER, we conduct prototype-based experiments under multiple settings. We first independently test the tethering and communication subsystems under controlled conditions, then evaluate their performance under interference and in the integrated communication and tethering setting. We further test the system's EMI resistance, perform field studies with real UAV deployments, and finally design an emulation framework grounded in real-world performance metrics to assess the performance attainable with advanced engineering implementations.

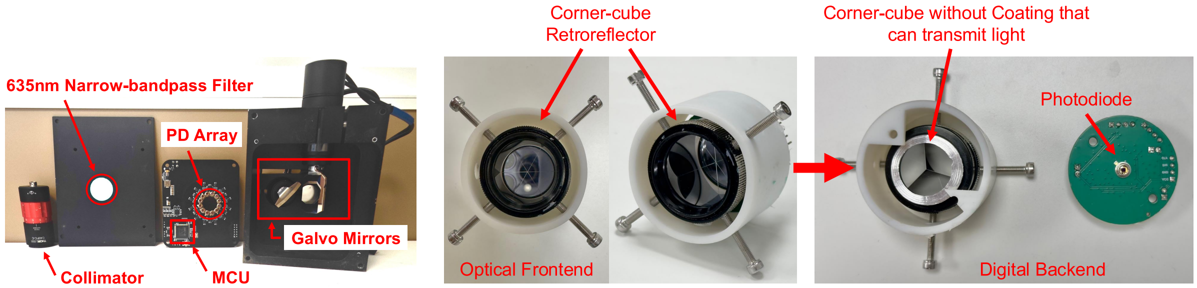

(a) Anchor.

(b) Node (front and back).

Fig. 4: Taken-apart prototype of LIGHTRIDER.

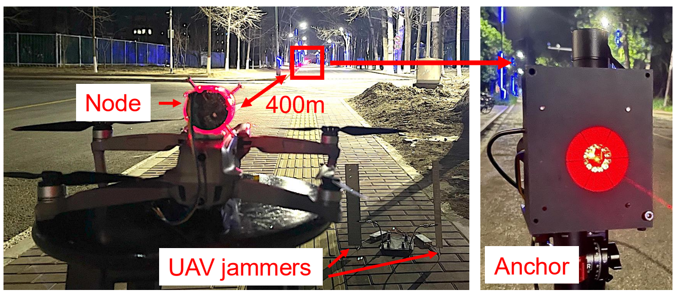

Fig. 5: Experimental Setup.

A. Experimental Setup

We evaluate LIGHTRIDER using our prototype implementation with a testbed illustrated in Fig. 5. For experiments not involving tethering, the Anchor and Node are mounted on tripods. Unless otherwise specified, the Node directly faces the Anchor in an outdoor road environment at night under streetlight illumination.

For tethering performance evaluation, we characterize UAV motion using angular velocity rather than linear velocity, because this metric intrinsically combines the UAV's linear velocity and its distance from the Anchor, directly determining the tracking performance required at the Anchor end. For example, a UAV at 100 m moving at 30 m/s requires about 17.2°/s angular tracking velocity, while a UAV at 1 m moving at 1 m/s requires 57.3°/s angular tracking velocity.

Our primary evaluation metrics include the bit error rate (BER) of decoded data at the Node for assessing the communication subsystem, and the SNR of signals received by the PD array at the Anchor for evaluating tethering performance. Note that tethering is successful as long as the Anchor can receive the reflected signal continuously.

B. Experimental Results

Tethering Performance. We evaluate tethering performance by mounting the Node on a rail system (maximum speed 1 m/s) and varying its distance from the Anchor. As shown in Fig. 6d (where distance and angular velocity on the vertical axis correspond one-to-one), the subsystem supports angular velocities up to 57.3°/s and maintains stable tethering to 150 m. Although SNR can still be measured at 160 m, continuous tethering is not sustained.

Communication Performance. We evaluate the communication subsystem at different data rates and distances while isolating tethering effects by fixing the transmitter and receiver on optical benches. At each distance, we send 200 packets (16 bits each) at various link rates and compute the BER at the Node. As shown in Fig. 6a, the system supports reliable communication (zero BER) up to 380 m at 10 Kbps.

Ambient Light and Weather Condition. We measure the system's robustness in diverse environments with interference, including clear daytime conditions during late afternoon and dense artificial fog scenarios. As shown in Fig. 6b and Fig. 6e, the communication and tethering ranges under sunlight decrease to 150 m and 120 m, respectively. This degradation primarily stems from intense solar radiation elevating the PD's dark current, thereby reducing SNR. In dense fog, the tethering range further diminishes to 70 m, mainly due to substantial laser attenuation caused by suspended water droplets and particulate matter.

Integrated Communication and Tethering. We further evaluate the performance of the system with integrated communication and tethering functions. As depicted in Fig. 6c, the integrated system achieves reliable operation up to 100 m, representing a 33.3% reduction compared to the maximum tethering distance of 150 m.

PD Array Microbenchmarking. To evaluate the impact of PD array configuration on tethering performance, we compare systems equipped with 3-, 6-, and 12-element PD arrays, with all PDs uniformly distributed on a common circumference. As shown in Fig. 6f, the maximum tracking distance increases with the number of PDs, because more PDs enable a more accurate estimation of the reflected beam center, thereby enhancing the beam-steering accuracy.

EMI Resistance. To evaluate the system's EMI resistance, we follow a standard methodology [27] by employing commercial drone jammers to create controlled EMI. Two 30 W jammers operating at 2.4 GHz and 5.8 GHz are placed 1–5 m from a DJI Air 2S UAV equipped with the Node. Across all tested distances, the UAV loses connectivity with its RF controller, whereas our optical system maintains reliable communication with zero BER.

Comparison with SOTA. The closest state-of-the-art (SOTA) system to our system is Lasertag [17], which uses LED-

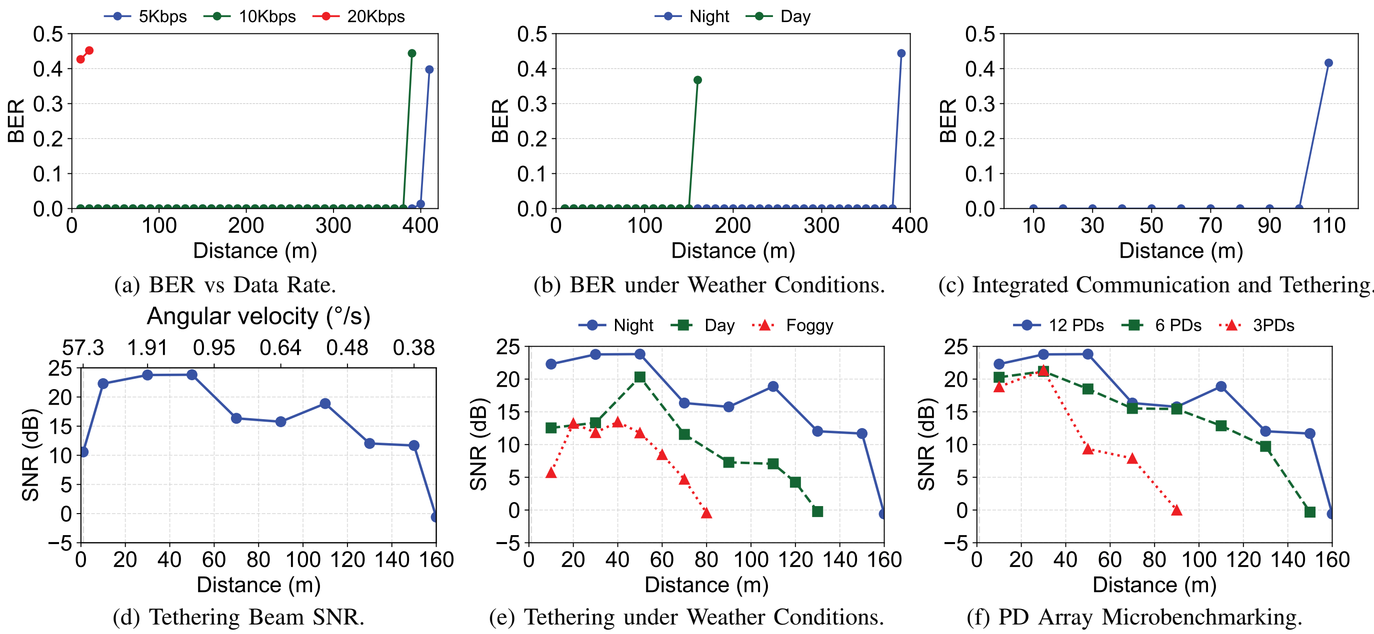

(a) BER vs Data Rate. (b) BER under Weather Conditions. (c) Integrated Communication and Tethering.

(d) Tethering Beam SNR. (e) Tethering under Weather Conditions. (f) PD Array Microbenchmarking.

Fig. 6: Performance Experiments.

illuminated, camera-based tracking of passive retroreflective markers for meter-scale mobile laser tethering. In contrast, LIGHTRIDER targets outdoor UAV-ground communication in EMI-prone environments and adopts a PD-array-based optical self-feedback loop with a coaxial design for long-range operation. Under the shared tethering metrics reported by both systems, LIGHTRIDER improves the tethering range from 6 m to 150 m (25×) and the supported angular velocity from 47°/s to 57°/s (21% increase). Communication metrics are less directly comparable because LIGHTRIDER directly evaluates end-to-end communication under UAV flight, whereas Lasertag reports communication feasibility by mapping mobile target-side PD measurements to the BER of a separately calibrated stationary 1 Gbps OOK link, where packets are generated by an arbitrary waveform generator, captured with an oscilloscope, and decoded offline in MATLAB.

Weight and Power. We use Monsoon [28] and a high-precision scale to accurately measure the power consumption and weight of the Node. The results show that the Node consumes only 140 mW of power and weighs 58.5 g, enabling the Node to be easily integrated into UAVs.

C. Emulation Results

Although our prototype demonstrates robustness in real-world experiments, it still falls short of the kilometer-scale communication distances typically required in practical UAV applications. This limitation mainly arises from the laser beam collimation performance and the galvanometer mirror control precision. Although both can be improved using commercial high-end components, they are not integrated into our prototype due to instrument availability. To assess the potential of a hardware-upgraded system, we build a high-fidelity emulator calibrated with the PD array layout, sampling rate, Gaussian-modeled laser beam properties, environmental noise, and the implemented communication and tethering algorithms. The emulator supports emulated node motion along specified trajectories at various distances, allowing us to explore performance under enhanced hardware configurations.

To verify emulator fidelity, we first configure it to match the prototype. Under this setting, it reproduces the 150 m tethering distance observed in experiments. Comparing tethering SNR at various distances with the measurements in Fig. 6d, we find the SNR difference is within 5 dB across all points, indicating that the emulator closely reflects the behavior of the real system.

Using the validated emulator, we then explore the impact of higher galvo control precision and improved optical collimation. As shown in Fig. 7a and Fig. 7b, both increasing the DAC resolution and using a higher-performance collimator extend the tethering range and improve SNR. Furthermore, when both enhancements are applied simultaneously, as shown in Fig. 7c, the emulated system sustains an SNR above 16 dB for distances up to 1200 m with Node mobility of 30 m/s. These results indicate that, with commercially available higher-grade components, our design can be scaled to more than 10x the operational range of the current prototype.

D. Field Study with Real UAV Deployment

To validate the operational capability of LIGHTRIDER in real UAV scenarios, we integrate the Node into a DJI Air 2S and conduct full-system tests. The UAV is manually flown along random trajectories at an approximate distance of 60 m from the Anchor. IMU data indicate a maximum speed of 6.2 m/s (5.9°/s) and a peak acceleration of 9.6 m/s^2. Even under these high-speed and unpredictable motions, LIGHTRIDER maintains a stable communication link with zero BER.

VII. DISCUSSION

Data Rate. The 10 Kbps rate of our prototype may seem to underutilize laser links, but it is primarily limited by non-

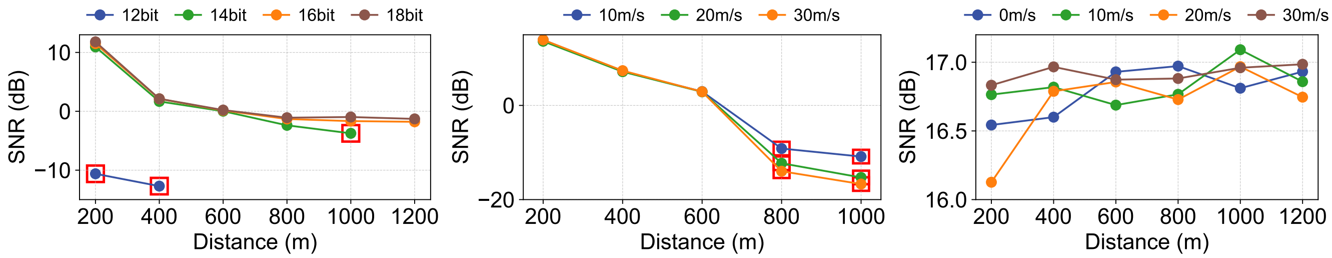

(a) Higher Control Precision. (b) Enhanced Optical Collimation. (c) With Both Optimizations.

Fig. 7: Emulation Results: The points enclosed by red boxes indicate tethering failure.

optimized optical switches, restricted PD bandwidth, and a fixed OOK modulation scheme. Crucially, data rate is orthogonal to our main goal: robust laser tethering under high mobility, which is fundamentally decoupled from link bandwidth and differs from most high-speed laser communication work focused on static scenarios. Even with our simple hardware and software, the tethering link provides sufficient SNR for data transmission. Future work can pair our tethering mechanism with higher-performance laser communication systems to overcome the current rate limitation.

Higher Mobility and Kilometer-scale Distance Support. Our experimental mobility evaluation is constrained by the sliding rail's maximum speed, which is lower than typical UAV velocities. Nonetheless, we demonstrate accurate tethering at multiple distances, which is a more critical metric since system performance is fundamentally bounded by angular rather than linear velocity. The achieved 57°/s satisfies the mobility requirements of most UAVs, as further confirmed by our field experiment on a real UAV. The observed range limitation mainly arises from engineering imperfections of the current prototype. Using emulation, we show that with a higher-precision GM and an improved optical frontend, our design can support kilometer-scale ranges comparable to SOTA laser communication systems.

Real-world Environmental Effects. Environmental factors, such as ambient sunlight and artificial light, introduce background noise and degrade SNR, while weather conditions like rain, fog, and snow impair laser links through scattering, absorption, and attenuation. Our experiments show that sunlight reduces effective range to 120 m in daylight, and that dense fog further reduces the range to about 70 m due to severe attenuation. To improve robustness, we propose: (1) using an infrared laser, which is less affected by atmospheric absorption and scattering and thus more resilient to adverse weather, and (2) increasing laser power to compensate for strong attenuation. Migrating to infrared mainly requires wavelength-matched emitters, photodiodes, and optical filters, while the tracking precision is still primarily determined by the received SNR and beam quality.

Duplex Communication. The current LIGHTRIDER design supports unidirectional communication from the Anchor to the Node, consistent with many laser communication systems. However, for UAV applications, we consider bidirectional communication crucial, as an uplink from UAV to ground can deliver sensor data (e.g., video, telemetry), and acknowledgments on the reverse path can improve reliability. Achieving duplex operation is nontrivial. A straightforward symmetric design with a laser transmitter and galvo mirrors on the UAV is generally impractical due to weight and power constraints. A more promising direction is to integrate a liquid crystal shutter (see §VIII) into the existing Node, with about 10 grams additional weight and a minimum power consumption of only sub-mW [29], enabling it to both reflect and modulate the Anchor 's laser in a self-aligned manner.

Initialization and Failure Recovery. LIGHTRIDER mainly targets the steady-state regime after the optical tether is established, with emphasis on in-flight tracking and link maintenance. Initialization and recovery from complete link interruption are not fully automated in the current design, because once optical feedback is lost, the Anchor cannot determine the correct steering direction. In such cases, the UAV is expected to cooperatively hover and roughly align with the Anchor until the Node re-enters the detectable region, after which closed-loop tethering resumes. Fully automated initialization and recovery remain future work.

VIII. RELATED WORK

Laser Tethering. Conventional laser tethering for inter-satellite or ground-to-space communication has relied on heavy electromechanical setups and complex telescopes, incurring weight and complexity challenges [30], while lighter solutions often sacrifice power or precision [31]. Mobile laser communication has used beacon lights, retroreflectors, cameras , and PDs at both anchor and node for short-range (<10 m) applications [17]. Our design instead relies solely on the laser itself for position feedback, removing the need for beacon lights and supporting both long-distance and high-mobility operation without the trade-offs of prior methods.

PD Array for Communication and Sensing. In visible light communications, PD arrays are commonly utilized as optical antenna arrays to receive concurrent channels to enhance data rate [32]. PD array can also be extended into wireless sensing applications, *e.g.,* for hand pose reconstruction [33]. While our methodology for beam spot positioning shares similarities with these applications in its use of PD arrays, it uniquely leverages the spatial distribution characteristics of laser beams to achieve precise beam spot position estimation for maintaining robust laser tethering.

Reflective Visible Light Communication. Reflective communication using visible light, notably through liquid crystal modulators, has emerged as a research focal point. The evolution from time-domain On-Off Keying to color-based and time-polarization techniques [34] shows significant advancement. Additionally, integrating Multi-user MIMO [35] and using digital micro-mirror devices or reflective displays [36] have pushed throughput to tens of kbps, highlighting the potential of (retro-)reflected visible light links. Contrary to these modulation-based methods, our Node design diverges by purely harnessing the reflective properties, without engaging in modulation with the retroreflector.

IX. CONCLUSION

We have demonstrated that a laser beam can inherently achieve tethering relying only on itself (while simultaneously supporting communication). The system resolves a long-standing chicken-and-egg problem in mobile laser applications. While laser-based communication offers unparalleled advantages in range, bandwidth, and EMI resistance, establishing a stable laser link conventionally required a higher-performance transmission medium for tethering. Our design successfully addresses this challenge by relying solely on the laser beam itself to establish and maintain a robust optical link, which concurrently supports communication. Through deployment on a rapidly moving UAV, we have further validated the effectiveness of this purely laser-based tethering approach. This insight paves the way for broader adoption of laser communication in mobile applications, unlocking new possibilities for high-performance, EMI-resistant wireless systems in dynamic environments.

REFERENCES

[1] U. R. Mogili and B. Deepak, "Review on application of drone systems in precision agriculture," *Procedia computer science*, 2018.

[2] R. Kellermann, T. Biehle, and L. Fischer, "Drones for parcel and passenger transportation: A literature review," *Transportation Research Interdisciplinary Perspectives*, 2020.

[3] M. Miron, D. Whetham, M. Auzanneau, and A. Hill, "Public drone perception," *Technology in Society*, 2023.

[4] A. J. K. Tsui and N. T. Ellis, "Boy injured after orlando holiday drone show," https://edition.cnn.com/2024/12/23/us/orlando-holiday-drone-show-ends-with-technical-difficulties-systems-falling-from-the-sky/index.html.

[5] I. Boukabou and N. Kaabouch, "Electric and magnetic fields analysis of the safety distance for uav inspection around extra-high voltage transmission lines," *Drones*, 2024.

[6] Y. Wang, L. Ma, and Z. Meng, "Effects of uwb electromagnetic pulse on uav data link system," in *2019 IEEE 6th International Symposium on Electromagnetic Compatibility (ISEMC)*, 2019.

[7] DJI, "Datalink 3," https://www.dji.com/datalink-3?backup_page=index.

[8] J. Wu, R. Liu, and S. Zhao, "The cognitive communication based anti-jamming method for uav swarm communication," in *IOP Conference Series: Materials Science and Engineering*, 2020.

[9] S. Park, H. T. Kim, S. Lee, H. Joo, and H. Kim, "Survey on anti-drone systems: Components, designs, and challenges," *IEEE access*, 2021.

[10] H. Takano, D. Hisano, M. Nakahara, K. Suzuoki, K. Maruta, Y. Onodera, R. Yaegashi, and Y. Nakayama, "Visible light communication on led-equipped drone and object-detecting camera for post-disaster monitoring," in *2021 IEEE 93rd Vehicular Technology Conference (VTC2021-Spring)*, 2021.

[11] S. Sharma, R. Lica, V. Prasad, L. Mottola, and L. Ambroziak, "Acoustic side-channel communications for aerial drones with hum," in *ACM SenSys*, 2024.

[12] Y. Almadani, D. Plets, S. Bastiaens, W. Joseph, M. Ijaz, Z. Ghassemlooy, and S. Rajbhandari, "Visible light communications for industrial applications—challenges and potentials," *Electronics*, 2020.

[13] timbercon, "Fiber optics for unmanned aerial vehicles (uav)," https://www.timbercon.com/resources/fiber-optic-applications/fiber-optics-for-unmanned-aerial-vehicles-uav/.

[14] T. Singal, *Optical Fiber Communications: Principles and Applications*. Cambridge University Press, 2016. [Online]. Available: https://books.google.com.hk/books?id=_JheDwAAQBAJ

[15] A. Malik and P. Singh, "Free space optics: current applications and future challenges," *International journal of optics*, vol. 2015, no. 1, p. 945483, 2015.

[16] S. M. Walsh, S. F. Karpathakis, A. S. McCann, B. P. Dix-Matthews, A. M. Frost, D. R. Gozzard, C. T. Gravestock, and S. W. Schediwy, "Demonstration of 100 Gbps coherent free-space optical communications at LEO tracking rates," *Scientific Reports*, 2022.

[17] C. J. Carver, H. Schwartz, Q. Shao, N. Shade, J. Lazzaro, X. Wang, J. Liu, E. Fossum, and X. Zhou, "Catch me if you can: Laser tethering with highly mobile targets," in *USENIX NSDI*, 2024.

[18] P. G. Goetz, W. S. Rabinovich, R. Mahon, J. L. Murphy, M. S. Ferraro, M. R. Suite, W. R. Smith, H. R. Burris, C. I. Moore, W. W. Schultz *et al.*, "Modulating retro-reflector lasercom systems for small unmanned vehicles," *IEEE Journal on Selected Areas in Communications*, vol. 30, no. 5, pp. 986–992, 2012.

[19] M. A. Khalighi and M. Uysal, "Survey on free space optical communication: A communication theory perspective," *IEEE Communications Surveys Tutorials*, 2014.

[20] J. Alda, "Laser and gaussian beam propagation and transformation," *Encyclopedia of optical engineering*, vol. 999, pp. 1013–1013, 2003.

[21] STMicroelectronics, "Stm32h750vb high-performance and dsp with dp-fpu, arm cortex-m7 mcu with 128 kbytes of flash memory, 1mb ram, 480 mhz cpu, l1 cache, external memory interface, jpeg codec, hw crypto, large set of peripherals." [Online]. Available: https://www.st.com/en/microcontrollers-microprocessors/stm32h750vb.html

[22] "Photodiode lsipd-ul0.3." [Online]. Available: http://www.lightsensing.com/product236.html

[23] T. Instruments, "Opa2192 data sheet, product information and support — ti.com." [Online]. Available: https://www.ti.com/product/OPA2192

[24] S. Technologies, "S-9320 moving magnet capacitive position detector galvanometer scanner." [Online]. Available: http://www.sunny-technology.com/pro_con.aspx?type=25&id=846

[25] Thorlabs, "Thorlabs - c40fc-c achromatic fiber collimator, f = 40 mm, fc/pc, arc: 1050 - 1650 nm." [Online]. Available: https://www.thorlabs.com/thorproduct.cfm?partnumber=C40FC-C

[26] E. Moon, S.-W. Park, H. Chung, J.-Y. Lee, C. Bae, J.-W. Kim, J. Paek, and H. Kim, "Truncated corner cubes with near-perfect retroreflection efficiency," *Applied optics*, vol. 53, no. 33, pp. 7972–7978, 2014.

[27] T. Svimonishvili, E. K. Chua, and K. Y. See, "Susceptibility evaluation of commercial drone in harsh electromagnetic environment," in *2022 Asia-Pacific International Symposium on Electromagnetic Compatibility (APEMC)*, 2022.

[28] "Monsoonpowermonitor," http://www.msoon.com/LabEquipment/PowerMonitor.

[29] X. Xu, Y. Shen, J. Yang, C. Xu, G. Shen, G. Chen, and Y. Ni, "Passivevlc: Enabling practical visible light backscatter communication for battery-free iot applications," in *ACM MobiCom*, 2017.

[30] T. Schwander, R. Lange, H. Kämpfner, and B. Smutny, "Lctsx: first on-orbit verification of a coherent optical link," in *International Conference on Space Optics—ICSO 2004*, vol. 10568. SPIE, 2018, pp. 655–658.

[31] S. Janson and R. Welle, "The nasa optical communication and sensor demonstration program," 2013.

[32] K. Ying, H. Qian, R. J. Baxley, and S. Yao, "Joint optimization of precoder and equalizer in MIMO VLC systems," *IEEE Journal on selected areas in communications*, 2015.

[33] T. Li, X. Xiong, Y. Xie, G. Hito, X.-D. Yang, and X. Zhou, "Reconstructing hand poses using visible light," *ACM IMWUT*, 2017.

[34] S. K. Ghiasi, M. A. Z. n. Zamalloa, and K. Langendoen, "A principled design for passive light communication," in *ACM MobiCom*, 2021.

[35] K. Xu, C. Gong, B. Liang, Y. Wu, B. Di, L. Song, and C. Xu, "Low-latency visible light backscatter networking with retromumimo," in *ACM SenSys*, 2022.

[36] T. Xu, M. C. Tapia, and M. Zúñiga, "Exploiting digital micro-mirror devices for ambient light communication," in *USENIX NSDI*, 2022.